Metser reviews 2 approaches to ^{18}F-FDG PET prediction of prognosis in patients undergoing treatment for metastatic colorectal cancer and comments on the clinical investigation by Dimitrakopolou-Strauss and colleagues in this issue. . . . . ***Page 1428***

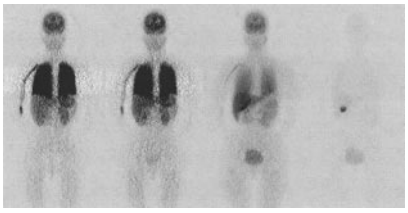

Thie provides perspective on standardized uptake value, the various methods of measuring it, and the influencing factors that limit its usefulness in comparisons—factors that Boellaard and colleagues specifically investigated and report in this issue. . . . . ***Page 1431***

Langen and Bröer trace the history of investigations into molecular transport mechanisms of radiolabeled amino acids for PET and SPECT, with special focus on the transport characteristics of ^{123}I-2-iodotyrosine and the investigation reported by Lahoutte and colleagues in this issue. . . . . ***Page 1435***

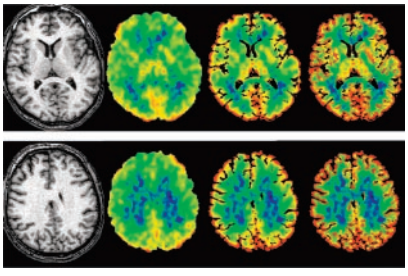

Tio and colleagues report on PET research comparing the results of intramyocardial VEGF gene therapy and laser treatment in reducing ischemia in patients with end-stage coronary artery disease and angina. . . . . ***Page 1437***

Nishimura and colleagues outline a simple method for superimposing the image of the coronary artery tree on 3D surface map images generated from gated myocardial perfusion SPECT, effectively superimposing radiography on scintigraphy in the evaluation of coronary artery disease. . . . . ***Page 1444***

Imabayashi and colleagues assess the potential advantages of artificial intelligence as an adjunct to visual interpretation in identifying patients with very early Alzheimer's disease. . . ***Page 1450***

Mamede and colleagues describe a novel method for quantification of nicotinic acetylcholine receptors in the human brain using ^{123}I-5IA SPECT and assess the suitability of this approach. . . . . ***Page 1458***

Giovacchini and colleagues use PET to evaluate the effects of healthy aging on brain incorporation of ^{11}C-arachidonic acid, before and after partial-volume correction, in both young adults and elderly individuals. . . . . ***Page 1471***

Dimitrakopoulou-Strauss and colleagues compare different quantification methods for use with ^{18}F-FDG PET in the prediction of individual survival in patients with metastatic colorectal cancer who are receiving chemotherapy with FOLFOX. . . . . ***Page 1480***

Poddar and colleagues report on an investigation on the effects of pretreatment with ursodeoxycholic acid, a choleretic agent, on the ability of ^{99m}Tc hepatobiliary scintigraphy to differentiate extrahepatic biliary atresia from neonatal hepatitis. . . . . ***Page 1488***

Brenner and colleagues evaluate the relationship between ^{18}F-fluoride bone metabolic measures obtained by nonlinear regression, Patlak analysis, and PET standardized uptake value for a wide range of normal and pathologic bone conditions. . . . . ***Page 1493***

Reinartz and colleagues compare advances in ventilation/perfusion lung scintigraphy and multislice spiral CT in patients with suspected pulmonary embolism. . . . . ***Page 1501***

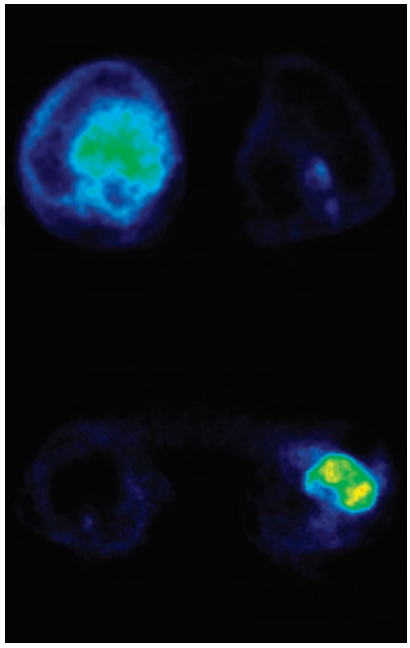

Torabi and colleagues describe the evolution of lymph node imaging techniques in nuclear medicine, from conventional anatomic modalities to molecular techniques in functional and physiologic assessment. . . . . ***Page 1509***

Boellaard and colleagues present the results of an experimental simulation study performed to determine the effects of noise, image resolution, and region-of-interest definition on the accuracy of standardized uptake values in ^{18}F-FDG PET. . . . . ***Page 1519***

Strauss and colleagues evaluate ^{18}F-FDG kinetics using compartment and noncompartment models of giant cell tumors and compare the results with gene expression data for a subgroup of patients. . . . ***Page 1528***

Taki and colleagues study ^{99m}Tc-annexin V uptake in rats after coronary occlusion and reperfusion to determine the timing and location of apoptotic cell death after reperfusion. . . . . ***Page 1536***

Schmitt and colleagues explore the successful results of radiation therapy with ^{177}Lu-DOTA-Tyr^3-octreotate in a human small-cell lung cancer cell line in mice and point to possible applications in humans. . . . . ***Page 1542***

de Keizer and colleagues study the effects of recombinant human thyroid-stimulating hormone on bone marrow in a group of 14 patients and discuss the relevance of this data to the use of the hormone as an adjunct in radioiodine therapy. . . . . ***Page 1549***

Lu and colleagues provide dosimetry estimates for ^{11}C-DASB, a selective radioligand for in vivo quantification of serotonin transporters, in human whole-body PET. . . . . ***Page 1555***

Green and colleagues investigate tracer kinetic models for ^{18}F-FHBG dynamic microPET data and noninvasive methods for determining blood time–activity curves in an adenoviral gene delivery model in mice. . . . . ***Page 1560***

Kang and colleagues report on data supporting the use of sodium iodide symporter–based gene therapy using β-emitting radionuclides in the management of patients with hepatocellular carcinoma. . . . . ***Page 1571***

Pain and colleagues propose the use of 2 positron-sensitive probes as an alternative to labor-intensive blood sampling for determination of input function after bolus injection of ^{18}F-FDG in small animals. . . . . ***Page 1577***

Chen and colleagues follow up on previous studies by assessing the efficacy of using tissue-to-plasma activity ratio as a simple alternative to dynamic imaging in determining net ^{18}F-FDG uptake during acute lung injury. . . . . ***Page 1583***

Lahoutte and colleagues characterize the interaction of ^{125}I-2IT and *h*4F2*hc*-*h*LAT1, the major transporter subserving system in growing cells. . . . ***Page 1591***

ON THE COVER

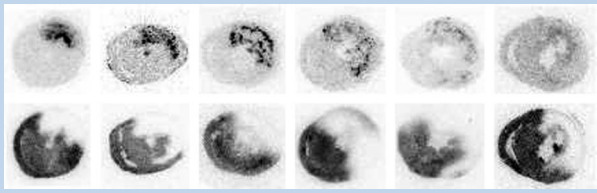

In these autoradiographs of heart slices from male Wistar rats, ^{99m}Tc-Annexin V shows the area of and intensity of apoptosis and ^{201}Tl shows the area at risk. ^{99m}Tc-annexin V uptake was significant in the area at risk and decreased with time after reperfusion. Significant uptake of ^{99m}Tc-annexin V is seen predominantly in the mid myocardium at 0.5 and 1.5 h after reperfusion and expands to the subendomyocardial and subepicardial layers and lateral border zone of ischemia at 6 h after reperfusion. Annexin V uptake is still observed after 1 d of reperfusion and decreases during the 3 d after reperfusion.